Available online at www.sciencedirect.com
SCIENCE DIRECT®
PERGAMON
International Journal of Heat and Mass Transfer 46 (2003) 3707–3716
International Journal of HEAT and MASS TRANSFER
www.elsevier.com/locate/ijhmt

A numerical study of turbulent flow and conjugate heat transfer in concentric annuli with moving inner rod

Shehua Huang [a,*], Chung-Hwan Chun [b]

[a] College of Water Resources and Hydropower, Wuhan University, Wuhan, 430072, China
[b] Department of Mechanical Engineering, Pohang University of Science & Technology, San 31, Hyoja-dong, Pohang, South Korea

Received 8 September 2002; received in revised form 15 January 2003

Abstract

A numerical study is conducted to investigate turbulent flow and conjugate heat transfer in a concentric annulus with a heated inner cylinder moving in the streamwise direction. A modified two-equation k–ε model with low Reynolds number treatment near wall is employed to model the Reynolds stress and turbulent thermal field which are based on Boussinesq's approximation. The governing equations are numerically resolved by means of a hybrid finite analysis method. A uniform inlet flow and thermal conditions are specified to consider the effects of entrance of both solid and fluid regions. For a constant Prandtl number of 6.99 of water flow, calculating results of the time-averaged streamwise velocity, turbulent viscosity and temperature field are obtained for the Reynolds numbers from 1.0×10^4 to 5.0×10^5, rod velocity ratio between 0 and 1.0, and the radius ratio ranging from 0.286 to 0.750. The parametric studies show that the bigger rod speed ratio or the radius ratio is, the temperature is higher within solid rod. For a certain absolute rod speed, temperature profile diminishes at both sides of solid rod and fluid as Reynolds number grows. Numerical results also show that compared with the case of $\beta = 0$ where solid rod is stationary, for large rod speed ratio the averaged axial velocity and turbulent viscosity profiles have substantial deformations, that is, the gradient of averaged axial velocity and turbulent viscosity near rod surface greatly reduced by the axial movement of solid rod.

Keywords: Conjugate heat transfer; Turbulent flow; Moving inner rod in concentric annuli; Nusselt number

1. Introduction

The problems of heat transfer and turbulent flow in concentric annuli with moving inner solid cores are encountered in various industrial applications, such as in manufacturing processes of extrusion and drawing, in cooling system of hot rolling for steel rod, in transportation of trains traveling in a long tunnel, and in nuclear reactors during emergency core cooling of nuclear fuel channels. In these cases, the moving core exchanges heat energy with the surrounding environment continuously, and the fluid flow can be either laminar or turbulent. In this paper we just study the turbulent flow and heat transfer phenomena.

Barrow and Pope [1] made a simple analysis of turbulent flow and heat transfer in the proposed railway tunnel between England and France. Shigechi et al. [2] and Lee and Shigechi [3] obtained analytical solutions for friction factors and Nusselt number for turbulent flow and heat transfer in concentric annuli with moving cores, using a modified turbulence model which is originally presented by Van Driest [4] and Reichardt [5]. Their study shows that the friction factor decreases while the Nusselt number increases with an increase in relative velocity of inner core to the averaged flow velocity. Lee and Kim [6] studied an inverted annular film boiling during an emergency core cooling of nuclear fuel channels which involved similar fluid flow and heat transfer phenomenon. Torii and Yang [7,8] numerically

* Corresponding author. Tel.: +86-27-67802210; fax: +86-27-67802310.
E-mail address: huangsh@public.wh.hb.cn (S. Huang).

0017-9310/03/$ - see front matter © 2003 Elsevier Ltd. All rights reserved.
doi:10.1016/S0017-9310(03)00170-4

Nomenclature

C_p	specific heat at constant pressure, J/kg K
C_μ, $C_{\varepsilon 1}$, $C_{\varepsilon 2}$	empirical constants of k–ε model
C_f	skin friction factor
k	dimensionless turbulent kinetic energy
Nu	Nusselt number
P	time-averaged pressure, Pa
Pr	Prandtl number
Pr_t	turbulent Prandtl number
U	axial mean velocity over gap of a annulus, m/s
u, v	time-averaged velocity components in axial and radial directions
x	dimensionless axial coordinate
y	dimensionless distance from wall
q	heat flux, W/m^2
r	dimensionless radial coordinate
Re	Reynolds number
R_1	inner radius of the annulus, m
R_2	outer radius of the annulus, m
Pe	Peclet number
T	time-averaged temperature, K
p	dimensionless pressure
v	molecular kinematic viscosity, m^2/s
v_t	dimensionless turbulent kinematic viscosity
σ_k, σ_ε	turbulent prandtl numbers for k and ε

Greek symbols

ε	turbulent energy dissipation rate
β	relative rod velocity or rod speed ratio
θ	dimensionless temperature
ρ	density, kg/m^3
α, α_t	molecular or turbulent thermal diffusivities, m^2/s
σ	radius ratio
λ	molecular thermal conductivity, W/m K
ϕ	variable

Subscripts

s	solid rod
f	fluid
t	turbulence
w, 1	inner wall, or solid rod surface
2	outer wall

investigated the effects of various parameters such as Prandtl number, relative velocity of inner core, radius ratio, on turbulent Couette flow and heat transfer in the same geometry as that in Shigechi's study [2], by using a version of low Reynolds number turbulence model by Launder and Shima [9]. It is found in their investigation that in the region near inner core, a reduction of velocity gradient due to its axial movement results in a decrease in heat transfer performance. Azouz and Shirazi [10] made an evaluation of several turbulence models for turbulent flow in concentric and eccentric annuli and their numerical results showed that a kind of mixing length model performs as well as low Reynolds two-equation model [11] except in the case where the annular gap is narrow.

It is worthwhile to notice that almost all of above researches are only involved in flow and heat transfer problems in annular fluid region for a given thermal boundary conditions, and no considerations are given to the heat conduction within the inner moving solid cores. In fact, it is often a basic requirement to know temperature distribution within moving solid rod in some applications such as hot rolling process where it is very hard to set a thermal boundary condition on the rod surface. Therefore, in both solid and fluid regions the heat transport phenomenon should be discussed together. When the interaction of heat conduction in solid rod with convection heat transfer in flow field must be considered simultaneously, such situations are referred to as conjugate flow and heat transfer problems. To authors' knowledge, there is seldom research done before on the conjugate heat transport phenomena in concentric annuli with moving inner cores [12].

The main objectives of this paper are to investigate the turbulent flow and conjugate heat transfer characteristics in concentric annuli with inner moving rod in the flow direction. A recently developed numerical scheme called hybrid finite analysis method (HFAM) [13] is used to discretize the governing equation sets for both flow and temperature fields in concentric annulus and the inner solid rod. A modified two-equation k–ε model with low Reynolds number treatment near walls [14] is employed to model the Reynolds stress and turbulent thermal field which are based on Boussinesq's approximation and Reynolds analogy respectively. Uniform flow and isothermal boundary conditions at both flow and solid rod inlets are specified to consider the effects of entrance region. Emphases of our researches are placed on the effects of movement of inner solid rod, various radius ratio and Reynolds number on thermal fields in whole domain and heat transfer rate on the surface of moving rod. Particularly, further attentions are paid on turbulent flow and temperature properties at outlet of both flow field and solid rod.

2. Governing equations and solution procedure

As shown in Fig. 1, we consider two dimensional axisymmetric turbulent convection flow and heat trans-

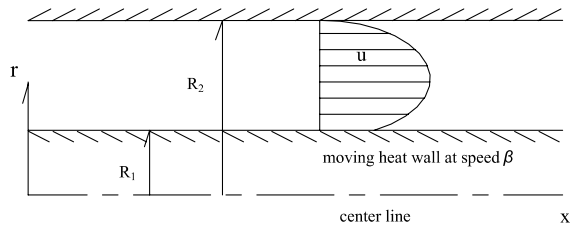

Fig. 1. Schematics of physical model and coordinate system.

fer coupled with a hot inner solid rod moving in a pipe concentrically. Assuming that effects of gravity are neglected as well as the effect of buoyancy due to temperature difference, the flow and heat transfer within both flow and solid areas can be regarded as a steady axisymmetric problem at stable operation condition. In two dimensional cylindrical coordinates, the averaged dimensionless governing equations for a steady turbulent annular flow of incompressible fluids and conjugate heat transfer of the translating solid rod are expressed as,

For fluid

$$\frac{\partial \bar{u}}{\partial x}+\frac{\partial \bar{v}}{\partial r}+\frac{\bar{v}}{r}=0, \tag{1}$$

$$\left(\bar{u}-2\frac{\partial v_t}{\partial x}\right)\frac{\partial \bar{u}}{\partial x}+\left(\bar{v}-\frac{\partial v_t}{\partial r}-\frac{1+v_tRe}{rRe}\right)\frac{\partial \bar{u}}{\partial r} = -\frac{\partial \bar{p}}{\partial x}+\left(\frac{1}{Re}+2v_t\right)\frac{\partial^2 \bar{u}}{\partial x^2}+\left(\frac{1}{Re}+v_t\right)\frac{\partial^2 \bar{u}}{\partial r^2} + \frac{1}{r}\frac{\partial}{\partial r}\left(rv_t\frac{\partial \bar{v}}{\partial x}\right), \tag{2}$$

$$\left(\bar{u}-\frac{\partial v_t}{\partial x}\right)\frac{\partial \bar{v}}{\partial x}+\left(\bar{v}-2\frac{\partial v_t}{\partial r}-\frac{1+2v_tRe}{rRe}\right)\frac{\partial \bar{v}}{\partial r} = -\frac{\partial \bar{p}}{\partial r}+\left(\frac{1}{Re}+v_t\right)\frac{\partial^2 \bar{v}}{\partial x^2}+\left(\frac{1}{Re}+2v_t\right)\frac{\partial^2 \bar{v}}{\partial r^2} + \frac{\partial}{\partial x}\left(v_t\frac{\partial \bar{u}}{\partial r}\right)-\frac{2}{Re}\frac{\bar{v}}{r^2}, \tag{3}$$

$$\left(\bar{u}-\frac{1}{Pr_t}\frac{\partial v_t}{\partial x}\right)\frac{\partial \bar{\theta}_f}{\partial x}+\left(\bar{v}-\frac{1}{rPe_f}-\frac{v_t}{rPr_t}-\frac{1}{Pr_t}\frac{\partial v_t}{\partial r}\right)\frac{\partial \bar{\theta}_f}{\partial r} = \left(\frac{1}{Pe_f}+\frac{v_t}{Pr_t}\right)\left(\frac{\partial^2 \bar{\theta}_f}{\partial x^2}+\frac{\partial^2 \bar{\theta}_f}{\partial r^2}\right). \tag{4}$$

For solid

$$-\beta\frac{\partial \theta_s}{\partial x}=\frac{1}{Pe_s}\left(\frac{\partial^2 \theta_s}{\partial x^2}+\frac{\partial^2 \theta_s}{\partial r^2}\right)+\frac{1}{Pe_s}\frac{\partial \theta_s}{r\partial r}. \tag{5}$$

We have taken fluid density ρ_f, averaged flow velocity U, the radius difference of inner and outer cylinders R_2-R_1, and averaged temperature difference between inner rod and cooling water at their entrance T_s-T_w, as four characteristic parameters used for normalization of above governing equations. The general non-dimensional temperature θ is defined as

$$\theta=\frac{T-T_w}{T_s-T_w}.$$

The Reynolds number Re, the fluid Peclet number Pe_f and solid Peclet number Pe_s are based on the following definitions:

$$Re=U(R_2-R_1)/v,$$
$$Pe_f=\rho_f C_{pf}U(R_2-R_1)/\lambda_f,$$
$$Pe_s=\rho_s C_{ps}U(R_2-R_1)/\lambda_s.$$

It should be specially pointed out that the energy Eq. (5) for solid rod is a little different from usual heat conduction equation. This is because the solid wire rod under cooling condition has an axial motion. In Eulerian reference frame it can be regarded as a kind of pseudo-fluid with a constant convection velocity of $\beta=u_0/U$, where u_0 is the absolute speed of moving rod. When the axial speed of solid rod is not small, the heat energy term from convection will be of great importance.

In above equation sets the Reynolds stress is modeled by Boussinesq's hypothesis, while turbulent heat flux is modeled according to Reynolds analogy, with a constant turbulent Prandtl number, $Pr_t=0.85$, used in this study. Within the framework of k–ε two-equation turbulence model, the turbulent viscosity v_t has the following relation with turbulence kinetic energy k and its dissipation rate ε,

$$v_t=C_\mu k^2/\varepsilon,$$

where C_μ is experimental constant. The turbulence kinetic energy k and its dissipation rate ε are determined from the following transport equations:

$$\left(\bar{u}-\frac{1}{\sigma_k}\frac{\partial v_t}{\partial x}\right)\frac{\partial k}{\partial x}+\left(\bar{v}-\frac{v_t}{r\sigma_k}-\frac{1}{\sigma_k}\frac{\partial v_t}{\partial r}\right)\frac{\partial k}{\partial r} = \frac{1}{Rek}\nabla^2 k+P_k-\varepsilon, \tag{6}$$

$$\left(\bar{u}-\frac{1}{\sigma_\varepsilon}\frac{\partial v_t}{\partial x}\right)\frac{\partial \varepsilon}{\partial x}+\left(\bar{v}-\frac{v_t}{r\sigma_\varepsilon}-\frac{1}{\sigma_\varepsilon}\frac{\partial v_t}{\partial r}\right)\frac{\partial \varepsilon}{\partial r} = \frac{1}{Re\varepsilon}\nabla^2\varepsilon+\frac{\varepsilon}{k}(C_{\varepsilon 1}P_k-C_{\varepsilon 2}\varepsilon), \tag{7}$$

where

$$Rek=Re\Big/\left(1+\frac{v_tRe}{\sigma_k}\right),\quad Re\varepsilon=Re\Big/\left(1+\frac{v_tRe}{\sigma_\varepsilon}\right),$$
$$\nabla^2=\frac{\partial^2}{\partial x^2}+\frac{\partial^2}{\partial r^2},$$

$$P_k = v_t \left\{ 2\left[\left(\frac{\partial \bar{u}}{\partial x}\right)^2 + \left(\frac{\partial \bar{v}}{\partial r}\right)^2 \right] + 2\left(\frac{\bar{v}}{r}\right)^2 + \left(\frac{\partial \bar{u}}{\partial r} + \frac{\partial \bar{v}}{\partial x}\right)^2 \right\}.$$

$(C_{\varepsilon 1}, C_{\varepsilon 2}, \sigma_k, \sigma_\varepsilon)$ are experiment constants whose values are taken as (1.44, 1.92, 1.0, 1.3) respectively. In the flow regions very close to walls, a two-layer approach [14] is used to consider the effect of viscous damping. In this method, a wall-distance-based turbulent Reynolds number Re_y is defined as

$$Re_y = y\sqrt{k}/v.$$

When $Re_y < 200$, the transport equations for turbulent dissipation rate ε is discarded, while the turbulent viscous coefficient is determined from

$$v_t = C_\mu l_\mu \sqrt{k},$$

where the above length scale is computed from

$$l_\mu = 0.41 C_\mu^{-3/4} y[1 - \exp(-Re_y/70)].$$

The above equations except for continuity equation can be written as unified form of 2D steady transport equation [13]:

$$2AC_1 \frac{\partial \phi}{\partial x} + 2BC_2 \frac{\partial \phi}{\partial r} = C_1 \frac{\partial^2 \phi}{\partial x^2} + C_2 \frac{\partial^2 \phi}{\partial r^2} + S, \tag{8}$$

where ϕ represents general unknown variable. A, B, C_1 and C_2 are coefficients of convection terms and diffusion terms respectively; S is source term. Detail forms of these coefficients for various equations are listed in Table 1. For these kinds of general convection–diffusion equations, a numerical scheme called HFAM [13] is employed to solve them. HFAM is a kind of improvement based on the traditional finite-analytic method (FA) which was firstly proposed by Chen et al. [18] and significantly developed by Chen and Chen [19]. Due to its built-in analytical nature, particularly for the advection-dominated flow problem, FA exhibits an excellent advantage of upwind shift that varies with the local flow direction and the grid-peclet number. However, the main drawbacks of FA are that its formulation is complex, and the finite-analytic coefficients involve one or more infinite series of exponential functions. Compared with FA, HFAM is a certain combination of interpolation bases of natural exponential functions on cells and eliminates the original infinite series in the finite-analytic coefficients. HFAM keeps not only FA's feature of upwind shift by itself and it also has greatly simplified the finite-analytic formulation. For steady flow HFAM is a scheme with second order accuracy. In a non-uniform rectangular mesh system, given $h_i = x_i - x_{i-1}$ and $k_j = r_j - r_{j-1}$ are step lengths of non-uniform grid at x and r directions respectively, five-point scheme of HFAM is as follows:

$$\begin{aligned} &-\frac{\bar{A}_{ij}}{\bar{h}_i^2 \sinh \bar{A}_{ij}} (e^{\bar{A}_{ij}} \phi_{i-1,j} + e^{-\bar{A}_{ij}} \phi_{i+1,j}) \\ &-\frac{\bar{B}_{ij}}{\bar{k}_j^2 \sinh \bar{B}_{ij}} (e^{\bar{B}_{ij}} \phi_{i,j-1} + e^{-\bar{B}_{ij}} \phi_{i,j+1}) \\ &+\left(\frac{2\bar{A}_{ij} C_{1ij}}{\bar{h}_i^2} c \tanh \bar{A}_{ij} + \frac{2\bar{B}_{ij} C_{2ij}}{\bar{k}_j^2} c \tanh \bar{B}_{ij} \right) \phi_{ij} = S_{ij}, \end{aligned}$$

where

$$\bar{A}_{ij} = A_{ij}\bar{h}_i + \frac{h_{i+1} - h_i}{2\bar{h}_i}, \quad \bar{h}_i = \frac{h_{i+1} + h_i}{2},$$

$$\bar{B}_{ij} = B_{ij}\bar{k}_j + \frac{k_{j+1} - k_j}{2\bar{k}_j}, \quad \bar{k}_j = \frac{k_{j+1} + k_j}{2}.$$

Calculations have been performed on a rectangular and staggered non-uniform gird system. The staggered grid is used to prevent from yielding non-physical jagged pressure field in final calculating results. Since pressure itself has no independent equation, mass continuity is

Table 1
HFAM coefficients of general convection and transport equations

	ϕ	$2AC_1$	$2BC_2$	C_1	C_2	S
x momentum	$\bar{u}$	$\bar{u} - 2\frac{\partial v_t}{\partial x}$	$\bar{v} - \frac{\partial v_t}{\partial r} - \frac{1 + v_t Re}{rRe}$	$\frac{1}{Re} + 2v_t$	$\frac{1}{Re} + v_t$	$-\frac{\partial \bar{p}}{\partial x} + \frac{1}{r}\frac{\partial}{\partial r}(r v_t \frac{\partial v}{\partial x})$
r momentum	$\bar{v}$	$\bar{u} - \frac{\partial v_t}{\partial x}$	$\bar{v} - 2\frac{\partial v_t}{\partial r} - \frac{1 + 2v_t Re}{rRe}$	$\frac{1}{Re} + v_t$	$\frac{1}{Re} + 2v_t$	$-\frac{\partial \bar{p}}{\partial r} + \frac{\partial}{\partial x}\left(v_t \frac{\partial \bar{u}}{\partial r}\right) - \frac{2}{Re}\frac{\bar{v}}{r^2}$
Fluid-energy	$\bar{\theta}_f$	$\bar{u} - \frac{2}{Pr_t}\frac{\partial v_t}{\partial x}$	$\bar{v} - \frac{1}{rPe_f} - \frac{v_t}{rPr_t} - \frac{1}{Pr_t}\frac{\partial v_t}{\partial r}$	$\frac{1}{Pe_f} + \frac{v_t}{Pr_t}$	$\frac{1}{Pe_f} + \frac{v_t}{Pr_t}$	0
Solid-energy	θ_s	β	$-1/(Pe_s r)$	$1/Pe_s$	$1/Pe_s$	0
k equation	K	$\bar{u} - \frac{1}{\sigma_k}\frac{\partial v_t}{\partial x}$	$v - \frac{v_t}{r\sigma_k} - \frac{1}{\sigma_k}\frac{\partial v_t}{\partial r}$	$1/Rek$	$1/Rek$	$P_k - \varepsilon$
ε equation	ε	$\bar{u} - \frac{1}{\sigma_\varepsilon}\frac{\partial v_t}{\partial x}$	$v - \frac{v_t}{r\sigma_\varepsilon} - \frac{1}{\sigma_\varepsilon}\frac{\partial v_t}{\partial r}$	$1/Re\varepsilon$	$1/Re\varepsilon$	$\frac{\varepsilon}{k}(C_{\varepsilon 1}P_k - C_{\varepsilon 2}\varepsilon)$

enforced by solving the pressure correction equation. The usual sequence of operations may be performed precisely in the same way as detailed by Patanker's SIMPLE procedure [15] for the staggered grid arrangement. In addition, the temperature equations in both flow and solid rod have been solved simultaneously in the calculations.

Now our attention is turned to computational domain and boundary conditions. As shown in Fig. 2, the total domain consists of two parts of flow area and solid rod. The flow field is the space between outer tube and inner rod. The radius difference of tube and rod is 5 mm which is also the length scale for parameter's normalization. The axial length of annulus is 200 mm which is according to the size of nozzle and guided tubes. We chose radius ratio, $\sigma = R_i/R_o$, as a variable to explore its effect on heat transfer. The range of radii ratio is from 0.285 to 0.833. For various radius ratio, grid sizes of 240×62, 240×65, 240×90, 240×100 and 240×120 are adopted in calculations respectively. The boundary condition for fluid flow is given as below.

At inlet of flow field, uniform boundary conditions for velocity, temperature, turbulent kinetic energy and its dissipation are specified by

$$u = 1.0, \quad v = 0, \quad \theta_f = 0, \quad k = 4.0 \times 10^{-4},$$
$$\varepsilon = C_\mu^{3/4} k^{3/2}/0.07.$$

If we assume flow and thermal fields are developed fully at the flow exit, secondary type boundary condition,

$$\frac{\partial \phi}{\partial x} = 0,$$

is used, where ϕ can be any unknown variable. On the still wall are non-slip velocity and constant temperature boundaries,

$$u = v = 0, \quad \theta_f = 0.$$

On the moving wall shared by both fluid and solid domain, similar non-slip velocity boundaries are considered as

$$v = 0; \quad u = \beta,$$

where β is rod relative speed. On both still and moving walls, turbulent kinetic energy and its dissipation are set as

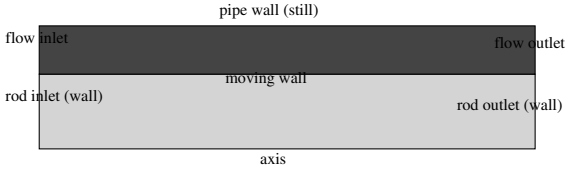

Fig. 2. Flow configuration and boundary types.

$$k = 0, \quad \partial\varepsilon/\partial r = 0.$$

For the heat coupling condition on the moving wall, the principle of heat flux conservation is applied to both fluid and solid sides according to Fourier law of heat conduction,

$$(\lambda_f + \rho_f C_{pf} \nu_t / Pr_t) \left.\frac{\partial \bar{\theta}_f}{\partial r}\right|_{r=R_1/(R_2-R_1)} = \lambda_s \left.\frac{\partial \theta_s}{\partial r}\right|_{r=R_1/(R_2-R_1)}.$$

In the area of solid rod, only heat boundaries need to be set. At rod inlet, a constant temperature is

$$\theta_s = 1.0$$

and at the exit of rod outlet, secondary type condition will be applied, that is,

$$\frac{\partial \theta_s}{\partial x} = 0,$$

which means that the effect of heat conduction of axial direction at the exit can be neglected. Along rod axis is the symmetric boundary condition due to axisymmetry of heat conduction,

$$\frac{\partial \theta_s}{\partial r} = 0.$$

3. Results and discussion

The numerical results and consequent discussions are divided into three parts to introduce. In part one is the verification of numerical procedure. Part two shows temperature fields in the total domain of physical model, along with thermal properties on the rod surface, say, Nusselt numbers. The definition of local Nusselt number is

$$Nu = \left.\frac{q(R_2 - R_1)}{(T_s - T_w)\lambda_f}\right|_{R=R_1} = -\left.\frac{\partial \theta}{\partial r}\right|_{r=R_1/(R_2-R_1)}.$$

Part three concerns temperature and averaged turbulent flow velocity profiles at outlet of the computation domain.

3.1. Validation of the numerical procedure

For validations of the simulation method used in this paper, at first some previous experimental results available in literature are used to compared with our calculation at the same flow and thermal boundary conditions. Since there is no experimental result on turbulent heat transfer in concentric annuli with moving inner cores, the comparisons can only be done for the situations where both outer wall and an inner rod are stationary. For an stationary annulus, under uniform wall heat flux and fully developed flow/thermal conditions Dalle Donne

and Meerwald [16] presented empirical formulations for the Nusselt number and friction factor at inner wall surface as follows,

$$Nu = 0.0181\sigma^{-0.2}(T_w/T_0)^{-0.18}Re^{0.8}Pr^{0.4}, \quad (9)$$

$$C_f = 0.0615(1-\sigma)^{0.1}Re^{-0.22}. \quad (10)$$

Figs. 3 and 4 are comparisons of calculated results with above empirical formulations, where the calculated results are the values at outlet of flow region. As shown in Fig. 4, the numerical prediction for friction factor is in good agreement with formulation (9) and the experimental data by Nouri et al. [17]. Although our calculation of local Nusselt number does not superpose correlation (10) completely in Fig. 3, both of them have similar relationship to Reynolds number. The small difference between calculated results and empirical formulation (9) may result from the given normalized axial length of $x = 40$ which is still not long enough for turbulent flow and heat boundary to develop very much. Figs. 5 and 6 depict the numerical and experimental

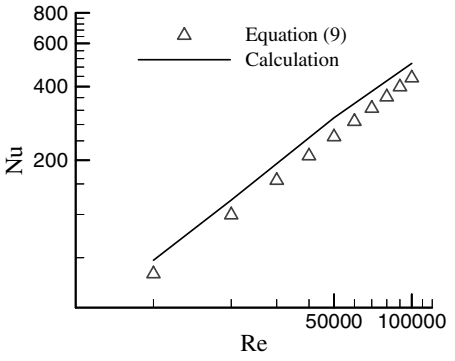

Fig. 3. Local Nusselt number on inner wall of a stationary concentric annulus at outlet of $x = 40$ for $Pr = 6.99$, $\sigma = 0.5833$.

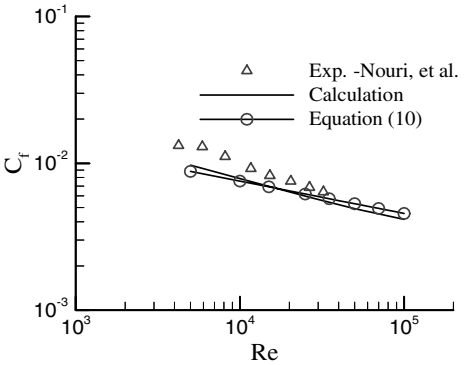

Fig. 4. Skin friction factor on inner wall of a stationary concentric annulus at outlet of $x = 40$ for $Pr = 6.99$, $\sigma = 0.5$.

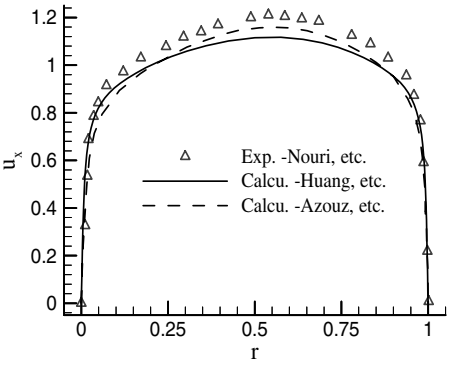

Fig. 5. Predicted axial velocity profile in a concentric annulus of radius ratio $\sigma = 0.5$ at outlet of $x = 40$ for $Re = 26,600$.

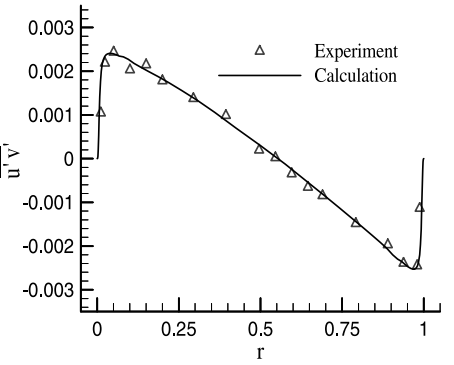

Fig. 6. Predicted Reynolds stress in a concentric annulus of radius ratio $\sigma = 0.5$ at outlet of $x = 40$ for $Re = 26,600$.

results of time-averaged axial velocity, Reynolds stress at flow outlet for Reynolds number of 26,600 in an stationary annulus with $\sigma = 0.5$. One can see from Fig. 5 that the experimentally measured velocity is a bit higher than those computed by Azouz and Shirazi [10] and us, and the velocity profile of our results is the flattest one among three results. It is demonstrated again that turbulent flow is indeed not so fully developed as required by the boundary condition at the flow outlet of $x = 40$. Fig. 6 illustrates that the calculated results of Reynolds stress are in perfect consistence with the experimental results.

3.2. Temperature fields in whole computation domain and thermal properties on rod surface

Computations of turbulent flow and temperature fields have been performed for liquid water with $Pr = 6.99$ and hot solid rod of plain carbon steel. Both materials' properties are listed in Table 2.

Figs. 7–9 show the predicted typical dimensionless temperature contours in both fluid and solid regions for

Table 2
Material's properties

	Kinematic viscosity v (m^2/s)	Density ρ (kg/m^3)	Thermal conductivity (W/m K)	Specific heat capacity C_p (J/kg K)
Liquid water	1.004×10^{-6}	998.2	0.6	4182
Solid plain carbon steel		7854	60.5	434

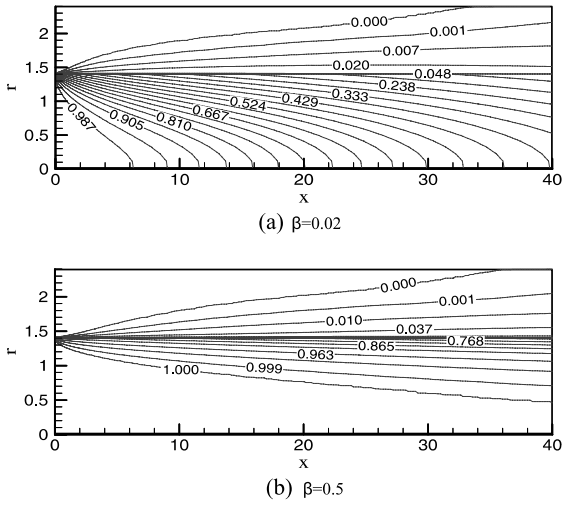

Fig. 7. Contours of temperature in meridian plane of a concentric annulus and a solid rod at $Re = 50,000$ and radius ratio $\sigma = 0.5833$ for various relative rod speed.

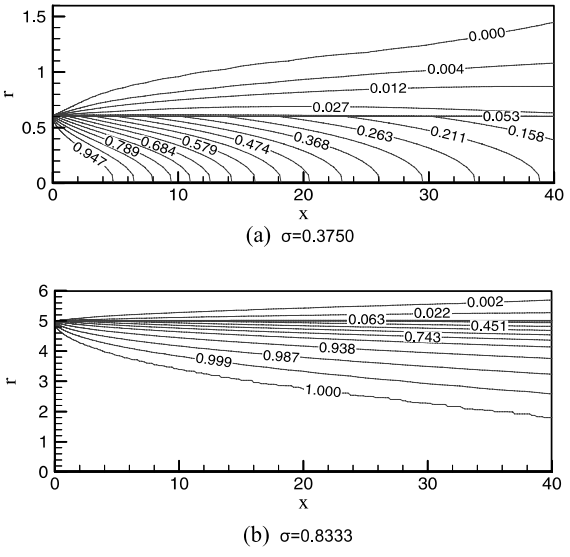

Fig. 8. Contours of temperature in meridian plane of a concentric annulus and a solid rod at $Re = 50,000$ and rod speed $\beta = 0.05$ for various radius ratio.

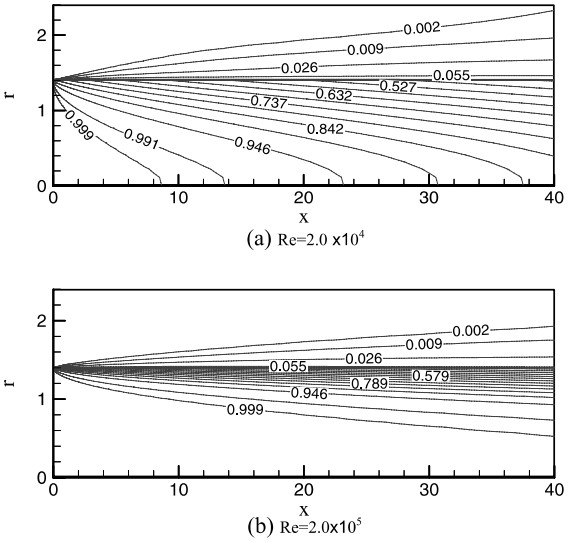

Fig. 9. Contours of temperature in meridian plane of a concentric annulus and a solid rod at $\sigma = 0.5833$ and rod speed $\beta = 0.1$ for various Reynolds number.

different combinations of rod velocity ratio, radio ratio and Reynolds number. From these results it is found that increases of rod velocity ratio, radio ratio and Reynolds number makes the isotherms to be close to the rod surface, which means temperature gradient as well as heat transfer on rod surface is stronger at large values of above parameters. However, these figures also illustrate that temperature contours keep higher values within solid rod in spite of strong heat transfer for large values of the three parameters respectively. Hence, if the other two parameters are fixed, the rod moves faster, the cooling effect is worse; the radius ratio is larger, the temperature is higher within solid rod; Reynolds number become bigger which implies more flow rate pass through annulus, the temperature in solid rod also attains higher values. It is easy to understand the results corresponding to the first two cases with larger rod speed and radius ratio, because large rod speed transports more heat energy into cooling area and increase of radius ratio means there is relatively more heat energy contained within solid rod. While an increase of Reynolds number also results in high temperature in solid rod. As expected, higher Reynolds number flow has enhanced convection of heat transfer in fluid region as

shown in Fig. 9(b), but in term of definition of rod relative velocity β, the absolute speed of rod motion increases as the increase of Reynolds number. So in this situation, the enhancement of heat convection due to higher Reynolds number does not counteract the increase of heat energy imported by rod movement.

Figs. 10 and 11 are calculated distributions of Nusselt number on the moving rod surface. For various axial positions rather than flow entrance, it is found that the effects of changing of any certain parameter, such as Reynolds number and rod relative velocity, on local Nusselt number are similar. So we just fix an axial position to discuss the results. In Fig. 10 for the range of $\beta = 0.01$–0.5, local Nusselt number is small at both small and large rod velocity ratio β. This is because the heat entering into flow field is relatively small for low rod speed, and flow velocity gradient becomes smaller for bigger rod speed at certain Reynolds number. When rod velocity ratio β is about 0.05–0.1, local Nusselt number reaches to its peak value. As shown in Fig. 11, an increase in Reynolds number causes an enhancement of local Nusselt number on rod surface.

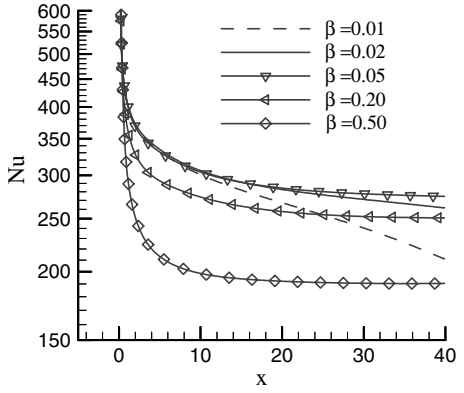

Fig. 10. Predicted distribution of Nusselt number on rod surface for various relative velocity of rod motion, $\sigma = 0.5833$, $Re = 50,000$.

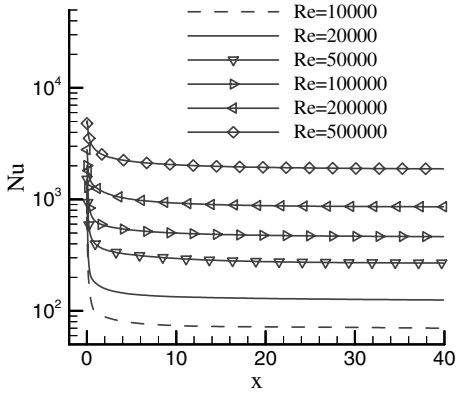

Fig. 11. Predicted distribution of Nusselt number on rod surface for various Reynolds number, $\sigma = 0.5833$, $\beta = 0.1$.

3.3. Temperature and averaged turbulent flow velocity profiles at outlet of the computation domain

Now let us concern with the flow and thermal properties at outlet of computation domain. Figs. 12–14 depict the variations of temperature profile along radial direction at outlet of flow and solid rod for different Reynolds number, relative speed of solid rod to average velocity of fluid and radius ratio of the rod to the outer cylinder respectively. Fig. 12 illustrates the effect of rod relative speed on temperature at outlet of both solid rod and fluid and an increase in rod relative speed results in a higher temperature in solid rod. When the moving speed of rod is big, a large radial temperature gradient forms at both sides of fluid and solid rod, which is, to some extent, helpful to enhance heat transfer on rod surface. However, this enhancement is not strong enough to counteract the increased heat flux due to the increment of rod speed. For a fixed rod absolute speed, as shown in Fig. 13, temperature profile diminishes at both sides of solid rod and fluid as Reynolds number grows. Temperature profiles along radial direction at outlet of rod and fluid for various radius ratio are shown in Fig. 14, which demonstrates that the larger a radius ratio is, the higher temperature is obtained in solid rod. For large radius ratio, temperature profile in solid rod tends to become uniform, which means less cooling effect of solid rod.

At last, our discussion is turned to the flow properties of averaged axial velocity and turbulent viscosity at flow outlet. Fig. 15 illustrates the radial profiles of time-

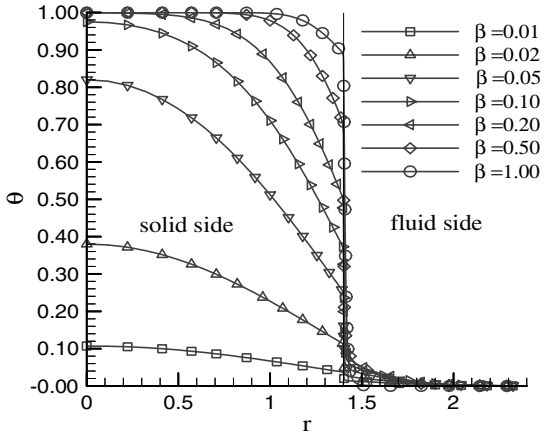

Fig. 12. Predicted non-dimensional temperature profile at outlet of flow and solid rod for various rod speed ratio ($\sigma = 0.5833$, $Re = 50,000$).

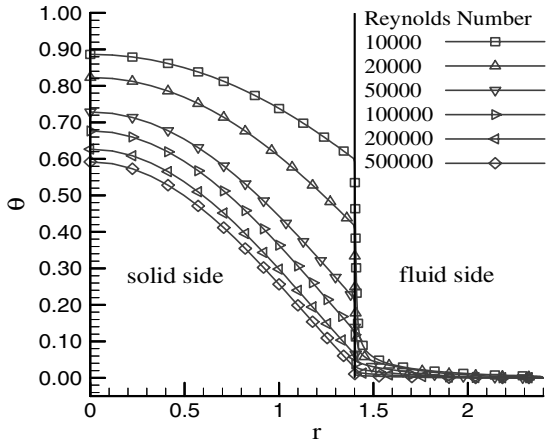

Fig. 13. Predicted non-dimensional temperature profile at outlet of flow and solid rod for various Reynolds number, ($\sigma = 0.5833$, $\beta U = 0.1$ m/s).

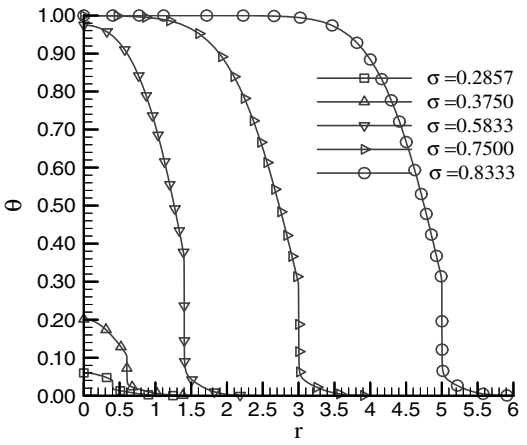

Fig. 14. Predicted non-dimensional temperature profile at outlet of flow and solid rod for various radius ratio ($\beta = 0.1$, $Re = 50,000$).

averaged dimensionless axial velocity for different rod speed ratio β. It is found that as β goes up, the peak value of axial velocity moves left toward the rod surface, with the axial velocity in the center region being decreased. Compared with the case of $\beta = 0$ where solid rod is stationary, for large rod speed ratio the averaged axial velocity profile has a substantial deformation. This implies that the gradient of averaged axial velocity near rod surface greatly reduced by the axial movement of solid rod. While at the side close to outer wall, there is little influence of solid rod motion on the gradient of averaged axial velocity. Predicted non-dimensional turbulent viscosity at outlet of flow for different rod speed ratio β is shown in Fig. 16. The change of β seems no

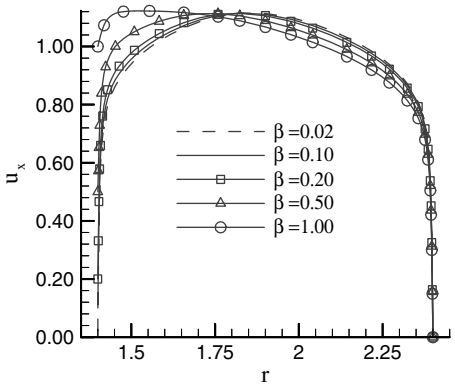

Fig. 15. Predicted non-dimensional streanwise velocity profile at outlet of flow for various rod speed ratio ($\sigma = 0.5833$, $Re = 50,000$).

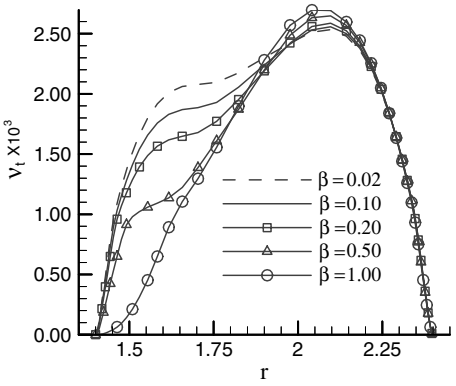

Fig. 16. Predicted non-dimensional turbulent viscosity at outlet of flow for various rod speed ratio ($\sigma = 0.5833$, $Re = 50,000$).

effect on turbulent viscosity in the vicinity of outer wall. However, as β increases, turbulent viscosity has enhanced in the center region inclined to outer wall and decreased in the area near rod surface. This behavior is in accordance with the variation of averaged axial velocity in Fig. 15.

4. Conclusions

Numerical predictions have been performed for two dimensional axisymmetrical turbulent flow and conjugate heat transfer in a concentric annulus with a heated inner cylinder moving in the streamwise direction. A modified two-equation k–ε model with low Reynolds number treatment near wall is employed to model the Reynolds stress and turbulent thermal field. The governing equations are numerically resolved by means of a HFAM. The following conclusions are derived from the present study.

For a steady conjugate heat transfer problem in both fluid and solid regions, a transformed form of heat conduction equation like Eq. (5) should be used to take into consideration of the movement of the solid body. This treatment is very convenient for general boundary conditions of computation to be introduced in whole domain. It is found from predictions that along streamwise direction as the axial distance away from flow inlet increases, local Nusselt number on rod surface decreases continuously for any flow conditions of our consideration.

The parametric studies show that increases of rod velocity ratio, radius ratio and Reynolds number have the isotherms in both fluid and solid regions to be close to the shared moving surface, which corresponds to larger heat transfer rate as well as larger temperature gradient on rod surface. If the other two parameters are fixed, the rod speed ratio is bigger, or the radius ratio is larger, the temperature is higher within solid rod. However, as Reynolds number increases, despite of correspondent enhancement of heat transfer on rod surface, the temperature in solid rod still attains higher values for a certain rod speed ratio. The temperature at flow and rod outlet comes down along with decrease of rod velocity and the radius ratio. For a given absolute rod speed, temperature profile at flow and rod outlet simply diminishes at both sides of solid rod and fluid as Reynolds number grows. Numerical results also show that compared with the case of $\beta = 0$ where solid rod is stationary, for large rod speed ratio the averaged axial velocity and turbulent viscosity profiles have substantial deformations, that is, the gradient of averaged axial velocity and turbulent viscosity near rod surface greatly reduced by the axial movement of solid rod. While at the side close to outer wall, there is little influence of solid rod motion on them.

Acknowledgement

The authors acknowledge the financial support that was received from Korea Science and Engineering Foundation (KOSEF).

References

[1] H. Barrow, C.W. Pope, A simple analysis of flow and heat transfer in railway tunnels, Heat Fluid Flow 8 (1987) 119–123.

[2] T. Shigechi, N. Kawae, Y. Lee, Turbulent fluid flow and heat transfer in concentric annuli with moving cores, Int. J. Heat Mass Transfer 33 (9) (1990) 2029–2037.

[3] Y. Lee, T. Shigechi, Heat transfer in concentric annuli with moving cores—fully developed turbulent flow with arbitrarily prescribed heat flux, Int. J. Heat Mass Transfer 35 (12) (1992) 3488–3493.

[4] E.R. Van Driest, On turbulent flow near a wall, J. Aerosp. Sci. 23 (1956) 1007–1011.

[5] H. Reichardt, Vollstandige darstellung der turbulenten geschwindigkeittsverteilung in glatten leitungen, Z. Angew. Math. Mech. 31 (1951) 208–219.

[6] Y. Lee, K.H. Kim, Inverted annular film boiling, Int. J. Multiphase Flow 13 (1987) 345–355.

[7] S. Torii, W.-J. Yang, A numerical study of turbulent Couette flow and heat transfer in concentric annuli, Int. J. Numer. Meth. Heat Fluid Flow 4 (1994) 367–377.

[8] S. Torii, W.-J. Yang, Numerical heat transfer in the thermal entrance region of turbulent parallel Couette flows in concentric annuli, Comput. Model. Simul. Eng. 2 (1997) 344–357.

[9] B.E. Launder, N. Shima, Second-moment closure for the near-wall sublayer: development and application, AIAA J. 27 (10) (1989) 1319–1325.

[10] I. Azouz, S.A. Shirazi, Evaluation of several turbulence models for turbulent flow in concentric and eccentric annuli, ASME J. Energy Res. Technol. 120 (1998) 268–275.

[11] C.J. Speziale, R. Abid, E.C. Anderson, Critical evaluation of two-equation models for near-wall turbulence, AIAA J. 30 (2) (1992) 324–331.

[12] I.T. Al-Zaharnah, B.S. Yilbas, M.S.J. Hashmi, Conjugate heat transfer in fully developed laminar pipe flow and thermally induced stresses, Comput. Meth. Appl. Mech. Eng. 190 (2000) 1091–1104.

[13] W. Li, Hybrid Finite Analysis Method of Incompressible Viscous Flow, Science Press, Beijing, China, 2000.

[14] H.C. Chen, V.C. Patel, Near-wall turbulence models for complex flows including separation, AIAA J. 26 (6) (1988) 641–648.

[15] S.V. Patankar, Numerical Heat Transfer and Fluid Flow, Hemisphere, Washington, DC, 1980.

[16] M. Dalle Donne, E. Meerwald, Experimental local heat transfer and average friction coefficient for subsonic turbulent flow of air in an annulus at high temperature, Int. J. Heat Mass Transfer 9 (1966) 1361–1376.

[17] J.M. Nouri, H. Umur, J.H. Whitelaw, Flow of Newtonian and non-Newtonian fluids in concentric and eccentric annuli, J. Fluid Mech. 253 (1993) 617–641.

[18] C.J. Chen, H. Naseri-Neshat, K.S. Ho, Finite-analytic numerical solution of heat transfer in two dimensional cavity flow, Numer. Heat Transfer 4 (1) (1981) 179–197.

[19] C.J. Chen, H.C. Chen, Finite-analytic method for unsteady two-dimensional Navier–Stokes equations, J. Comput. Phys. 53 (2) (1984) 209–226.